Journal of Membrane Science 549 (2018) 357–365

Contents lists available at ScienceDirect

Journal of Membrane Science

journal homepage: www.elsevier.com/locate/memsci

Biocatalytic and salt selective multilayer polyelectrolyte nanofiltration membrane

Nadir Dizge[a,b], Razi Epsztein[a], Wei Cheng[a,c], Cassandra J. Porter[a], Menachem Elimelech[a,*]

[a] Department of Chemical and Environmental Engineering, Yale University, New Haven, CT 06520-8286, USA
[b] Department of Environmental Engineering, Mersin University, Mersin 33343, Turkey
[c] State Key Laboratory of Urban Water Resource and Environment, School of Municipal and Environmental Engineering, Harbin Institute of Technology, Harbin 150090, China

ARTICLE INFO

Keywords:
Layer-by-layer membrane
Selective membrane
Biocatalytic membrane
Trypsin immobilization
Organic fouling

ABSTRACT

We used layer-by-layer (LbL) self-assembly to fabricate a polyelectrolyte (PE) nanofiltration membrane for salt rejection and to immobilize trypsin on the membrane outer layer for biocatalytic activity. Poly(ethylene imine) (PEI) and poly(diallyl dimethyl ammonium chloride) (PDADMAC) were used as cationic PE while poly(acrylic acid) (PAA) and poly(styrene sulfonate) (PSS) were used as anionic PE. The impact of PE type, number of PE bilayers, and PE concentration on the rejection of inorganic salts (NaCl, $MgCl_2$, Na_2SO_4, and $MgSO_4$) and protein (bovine serum albumin, BSA) was systematically investigated. A maximum rejection of 12.7%, 45.2%, 85.5%, 94.0%, and 100% of $MgCl_2$, NaCl, $MgSO_4$, Na_2SO_4, and BSA, respectively, was obtained by the PDADMAC-PSS membrane with four bilayers. Trypsin (TRY) was immobilized on the membrane surface by electrostatic attraction or covalent bonding to produce a biocatalytic membrane and to alleviate protein fouling. Important parameters for enzymatic activity, such as immobilization time, pH, temperature, salt concentration and type, as well as the reuse number and storage time were investigated to expound the mechanism of enzyme activity in the presence of salt and BSA. BSA was used as a model protein for organic fouling experiments, and flux decline rate of the membranes was determined. Our results show that LbL-modified membranes with covalent enzyme immobilization had the lowest protein fouling rate, which we attribute to the biocatalytic activity of the immobilized trypsin.

1. Introduction

Pressure-driven nanofiltration (NF) membranes have separation properties between ultrafiltration (UF) and reverse osmosis (RO) [1]. The “looser” active layer of NF membranes compared to RO membranes enables operation at relatively high-water flux and low pressure while maintaining efficient removal of pollutants and selective salt rejection [2–4]. The main rejection mechanisms of NF membranes, size (steric) and Donnan (charge) exclusions, result in varying removal capacity of different solutes based on their size and charge [5]. NF-based processes are increasingly used for wastewater reclamation and water treatment to remove a wide range of contaminants [6–11].

As in other membrane processes, the performance of NF membranes is hampered by fouling induced by organic substances such as proteins and soluble microbial products (SMP) [12–14]. Membrane fouling by proteins depends on a complex matrix of parameters, including membrane material, solution composition and pH, protein concentration, and operating conditions [15]. Electrostatic forces, hydrophobic interactions, and protein-protein interactions dictate the strength in which proteins bind to membrane surface or previously adsorbed proteins [16–18].

Bovine serum albumin (BSA) has served as a model protein in many previous investigations to explore UF and microfiltration (MF) membrane fouling [19–21]. However, investigations on NF membrane fouling by BSA are rather limited. Wang and Tang investigated protein fouling of polyamide NF membranes (NF 270 and NF 90) by BSA and demonstrated that electrostatic interactions played an important role during BSA fouling; these interactions may be partially attributed to the possible formation of disulfide bond between BSA molecules [22]. Another study showed that higher surface roughness promotes BSA adsorption on NF membranes [23].

The deposition of organic matter (e.g., proteins, carbohydrates, and lipids) on NF membranes decreases membrane water flux over time. Therefore, membranes must be chemically cleaned to eliminate the fouling layer and recover the water flux [24]. Commonly used cleaning agents such as chlorine, peroxide, and potassium permanganate have

* Corresponding author.
E-mail address: menachem.elimelech@yale.edu (M. Elimelech).

https://doi.org/10.1016/j.memsci.2017.12.026
Received 20 October 2017; Received in revised form 3 December 2017; Accepted 11 December 2017
Available online 12 December 2017
0376-7388/

strong oxidation capacity and can damage the membrane structure [25]. An enzyme-based biocatalytic degradation of organic foulants is an alternative methodology to mitigate membrane fouling. The use of enzymes can provide superior catalytic performance under mild conditions [26]. However, to reduce operating costs, enzymes would ideally be immobilized on the membrane for multiple use and for proactive prevention of biofouling. The main techniques for enzyme immobilization include adsorption, covalent binding, entrapment, and affinity immobilization [27,28].

Layer-by-layer (LbL) assembly of polyelectrolytes, initially proposed by Decher and Hong [29], is a simple technique to obtain a charged, multilayered, ultrathin membrane film on porous substrates such as UF membranes. The LbL assembly is prepared by immersing a substrate alternately into two oppositely charged polyelectrolyte solutions. Theoretically, different kinds of polyelectrolytes can be used to produce multilayered thin films. The LbL assembly technique can be potentially applied for pervaporation, gas separations, and water treatment [30–34].

To date, different types of polyelectrolytes and substrates have been explored to optimize salt rejection by the LbL self-assembly [35,36]. For example, Malaisamy and Bruening [37] used poly (ether sulfone) (PES) ultrafiltration membranes with different molecular weight cut-offs (MWCOs) as substrates for preparing polyelectrolyte composite NF membranes. They reported that LbL adsorption of polyelectrolytes on the PES substrate (MWCO of 50 kDa) produced a membrane with both high water flux and superior separation of salts and sugars from aqueous solutions. In another study, self-assembled alternating 60-layer pairs of PAH/PSS as cationic and anionic polyelectrolytes on a PAN/PET substrate resulted in high Na^+/Mg^{2+} and Cl^-/SO_4^{2-} selectivity of up to 112.5 and 45.0, respectively [38]. Ouyang et al. [39] used PAH and PSS as cationic and anionic polyelectrolytes for LbL assembly on PES substrates to prepare NF membranes. They obtained 40% rejection of NaCl at a feed solution concentration of 1 g/L (17 mM). At a lower feed concentration of 0.1 g/L (1.7 mM), the salt rejection increased up to 74%.

LbL assembly can be used as an effective and simple technique for enzyme immobilization on membranes. The resulting biocatalytic NF membrane can simultaneously digest proteins adsorbed on the membrane surface and serve as a selective barrier for different salts. Currently, systematic investigations of the preparation and performance of biocatalytic salt selective membranes via LbL self-assembly are limited [40,41]. Specifically, the antifouling performance of trypsin (TRY)-immobilized membranes in the presence of salt was not thoroughly addressed [28,42].

In this study, we fabricated a salt selective biocatalytic nanofiltration membrane with immobilized trypsin via LbL self-assembly. The selected conditions during the self-assembly procedure to achieve optimal salt selectivity and biocatalytic activity are discussed. The fabricated membrane exhibited high enzyme stability with a reduced fouling rate during BSA filtration.

2. Materials and methods

2.1. Materials and chemicals

Porous flat-sheet polysulfone (PSf) membrane with a 20 kDa molecular weight cut-off (MWCO) was supplied from Sepro and was used as a substrate for LbL self-assembly. Poly(ethylene imine) (PEI; M_w = 750,000 g/mol, 50 wt%), poly(diallyl dimethyl ammonium chloride) (PDADMAC; M_w = 150,000–200,000 g/mol, 20 wt%), and poly(allyl amine hydrochloride) (PAH; M_w = 450,000 g/mol, powder) were used in the LbL self-assembly as polycations and were purchased from Sigma-Aldrich. Poly(acrylic acid) (PAA; M_w = 100,000 g/mol, 35 wt%), and poly(sodium styrene sulfonate) (PSS; M_w = 70,000 g/mol, powder) were used as polyanions and were also purchased from Sigma-Aldrich. Glutaraldehyde (GA) solution (50 wt% in H_2O) was obtained from Sigma-Aldrich. The molecular structures of the polyelectrolytes and glutaraldehyde are shown in Fig. S1. Aqueous solutions of NaCl (Mallinckrodt Chemical Company), Na_2SO_4 (Acros Organics Chemical Company), $MgCl_2{\cdot}6H_2O$ (J.T Baker Chemical Company), $MgSO_4{\cdot}7H_2O$ (J.T Baker Chemical Company), and bovine serum albumin (BSA, Merck) were prepared with deionized water and used as feed solutions in the membrane experiments. NaCl solution (0.2 M) was used as solvent to dissolve the polyelectrolytes and to rinse the membranes during LbL self-assembly. The deionized water used in the experiments was provided by Milli-Q ultrapure water system (Academic A-10, resistance 18.2 MΩ cm).

Trypsin from porcine pancreas lyophilized powder, type II-S (EC 3.4.21.4 and 1000–2000 units/mg dry solid) with molecular weight of 23.8 kDa was purchased from Sigma-Aldrich. Nα-Benzoyl-DL-arginine p-nitroanilide hydrochloride (BAPNA) and trizma® hydrochloride buffer solution (pH 8.0) were also provided from Sigma-Aldrich. Trypsin hydrolyzes BAPNA to Nα-benzoyl-L-arginine and p-nitroaniline (p-NA) (Fig. S2). All chemical reagents were of analytical grade.

2.2. Modification of polysulfone membrane via LbL self-assembly

Prior to membrane modification, PSf substrate was immersed in 25% isopropanol solution for 30 min. Then, the membrane was rinsed with deionized water three times (each rinse for 30 min) and soaked in water overnight to remove impurities like preservative agents and dust. All polyelectrolytes were dissolved in 100 mL NaCl solution (0.2 M) and stirred for 3 h to achieve homogeneity. The membrane was carefully cut into a suitable size and clamped tightly in a specially-designed rectangular Teflon frame with only the active surface facing up and exposed. During LbL assembly, it was within this frame that solutions were poured over the membrane and gently swirled on a shake plate for what we subsequently term “contact” with the membrane.

The LbL assembly procedure (Fig. S3) started with contact of the aqueous solution of cationic polyelectrolyte with the active surface of the PSf substrate for 30 min. Excess cationic polyelectrolyte solution was rinsed away by contacting the substrate surface with NaCl solution (0.2 M) for 30 min. Following the rinse, the anionic polyelectrolyte solution was contacted with the cationic polyelectrolyte-loaded PSf substrate for 30 min to obtain electrostatic attraction between the cationic and anionic polyelectrolyte molecules. After the excess anionic polyelectrolyte molecules were removed by immersing the membrane surface in NaCl solution (0.2 M) for 30 min, the first electrostatically assembled bilayer (one cationic and one anionic layer) was produced. Multiple bilayers were prepared by repeating the steps described above. All the composite membranes were prepared by the LbL self-assembly at a room temperature of 25 ± 1 °C.

Table 1 presents the experimental conditions applied to prepare and test composite membranes using the layer-by-layer self-assembly process. The prepared membranes were tested for salt and BSA rejection. The effect of polyelectrolyte type and the number of polyelectrolyte bilayers were investigated to understand the relationship between membrane structure/composition and salt/BSA rejection.

2.3. Preparation of biocatalytic membranes via LbL self-assembly

A schematic representation of the procedure for biocatalytic membrane preparation using LbL self-assembly is given in Fig. 1. PDADMAC-PSS membrane with four bilayers made by 500 mg/L polyelectrolyte solution was chosen for trypsin immobilization in order to obtain high salt rejection (Section 3.1). In order to covalently bind trypsin enzyme in the presence of glutaraldehyde, PAH polyelectrolyte was attached to the PDADMAC-PSS membrane using the same procedure for polyelectrolyte deposition described in Section 2.2. PAH contains amine groups that glutaraldehyde can rapidly react with to form a Schiff base (−C=N−) under mild conditions (room temperature and neutral pH). The PSS-PAH membrane was then incubated in glutaraldehyde solution

Table 1
Preparation and testing conditions for optimization of LbL self-assembly nanofiltration membranes. Two main independent parameters were varied, the type of polyelectrolytes used and the number of polyelectrolyte bilayers; one bilayer comprises one anionic and one cationic layer.

Varied independent parameter	Conditions				
	Type of polyelectrolytes	Number of polyelectrolyte bilayers	Polyelectrolyte conc. (mg/L)	Salt conc. (mM)	BSA conc. (mg/L)
Type of polyelectrolytes	Cationic: PEI or PDADMAC; Anionic: PAA or PSS	2	500	2	100
Number of polyelectrolyte bilayers	PDADMAC/PSS	2, 4, or 6	500	2	100

(2% (w/v)) with trizma-HCl buffer (0.1 M, pH 8.0 containing 0.02 M $CaCl_2$) for 2 h. The PSS-PAH-GA membrane was washed several times with the buffer to remove unreacted glutaraldehyde.

The PDADMAC-PSS and PSS-PAH-GA membranes (6 cm × 10 cm) were immersed in positively charged trypsin (isoelectric point, pH(I): 10.1) solution (100 mL, 1 mg/mL) for different immobilization times (Table 2) at 25 ± 1 °C to achieve both electrostatic (Fig. 1a) and covalent (Fig. 1b) immobilization of trypsin, respectively. After incubation with trypsin, the membrane was washed three times with trizma-HCl buffer. The amount of immobilized trypsin was determined by measuring the trypsin concentration in solution using the protein assay procedure described in Section 2.6. After immobilization, trypsin-immobilized membranes were stored until use in trizma-HCl buffer solution at 4 °C to protect the enzymes from autolysis.

Attenuated total reflectance Fourier transform infrared (ATR-FTIR) spectroscopy analyses (Thermo Nicolet 6700) were carried out in the range of 450–4000 cm^{-1} to compare the functional groups on membrane surfaces before and after trypsin immobilization.

Table 2
Immobilization time and solution conditions applied (i.e. pH, temperature and salt type) for activity measurements of free and immobilized enzyme.

Varied independent parameter	Conditions		
	Immobilization time (h)	pH	Temperature (°C)
Immobilization time	1, 2, 4, 6, 8, 24	8	25
pH	24	5, 6, 7, 8, 9, 10, 11, 12	30
Temperature (°C)	24	8	30, 40, 50, 60, 70, 80

The water contact angle of all membranes was measured by static contact angle measurements using a goniometer (OneAttension, Biolin

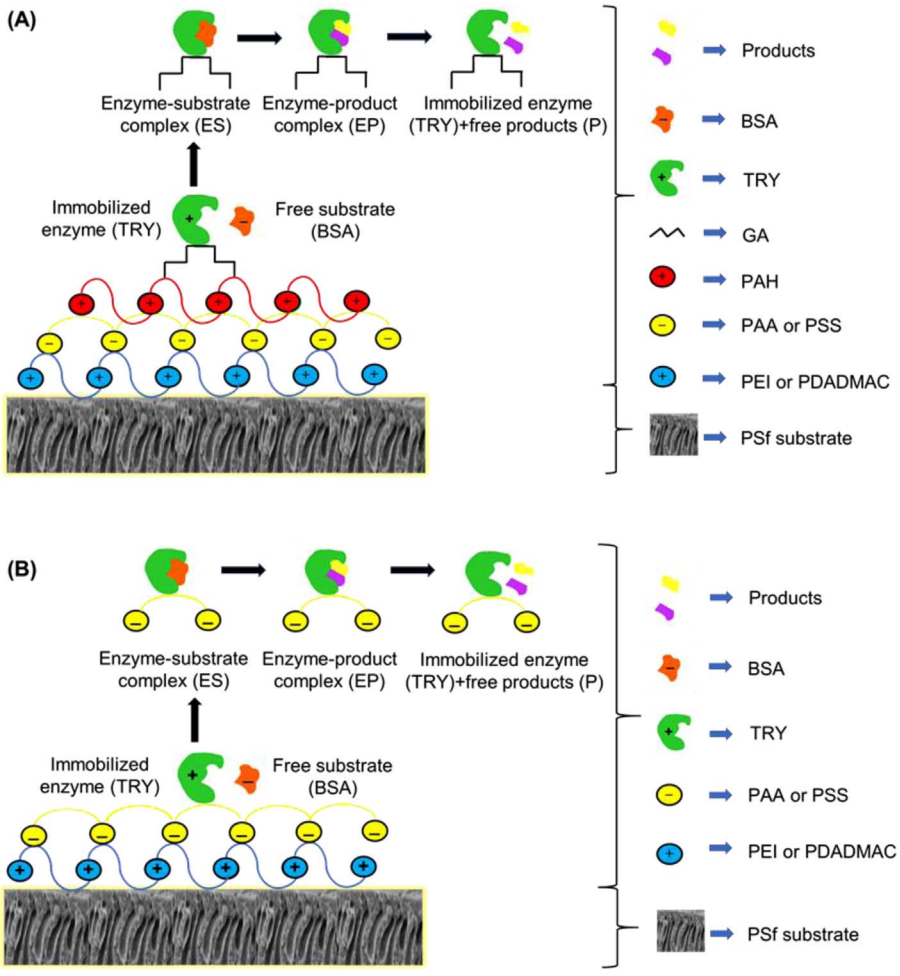

Fig. 1. Schematic representation of **(A)** covalent immobilization **(B)** physical immobilization of trypsin via LbL self-assembly.

scientific instrument) with the sessile drop method. Droplets of testing liquid (3 μL) were placed on three different locations on the sample surface, and the contact angle on the specimens was measured. Contact angle measurement was performed 5 s after dispensing 3 μL of the testing liquid on the membrane surface. The left and right contact angles were analyzed from the digital images by a post-processing software (OneAttension software).

The surface roughness of the pristine and modified membranes was determined by atomic force microscopy (AFM) analyses (Bruker Dimension Fastscan AFM). The average of the surface roughness values (R_a) was calculated as the standard deviation of all the height values within the given area. Small squares (0.5 cm × 0.5 cm) of dried samples were cut, and 1 μm × 1 μm areas were scanned in contact mode in air. For each sample, the average R_a value is given for three different regions scanned with 3.7 Hz scan rate.

2.4. Activity measurement of the biocatalytic membranes

Important parameters for obtaining high enzyme activity, such as pH, temperature, and presence of different salts, were investigated (Table 2). The effect of pH (5−12), temperature (30–80 °C), and salt type (NaCl, $MgCl_2$, Na_2SO_4, and $MgSO_4$ at 2 mM) on activity of free enzyme and biocatalytic membranes was tested using the specific activity assay procedure described below. We used citric acid-sodium citrate (pH 5.0, 6.0) and trizma-HCl (pH 7.0–12.0) to maintain various pH conditions during enzymatic activity.

The proteolytic activity of free and immobilized trypsin was determined by catalytic hydrolysis of BAPNA as a substrate according to a procedure described previously [28]. A 3 cm × 3 cm membrane coupon was soaked in 10 mL BAPNA solution. Specific activity assays were performed in a shaking incubator (VWR Scientific) at 25 rpm. After 30 min reaction time, the specific activity of trypsin (*SA*, μmol min^{-1} mg^{-1}) at different conditions was calculated using Eq. (1).

$$SA = \frac{A\ V}{t\ \varepsilon\ \ell\ m} \quad (1)$$

where A is the absorbance value of the product (p-NA) at 410 nm, V is the volume of sample (mL), t is the reaction time (min), ε is the extinction coefficient of p-NA at 410 nm (8.8 mM^{-1} cm^{-1}), l is the optical path (cm) and m is the amount of free/immobilized enzyme (mg). The activity of immobilized trypsin (μmol min^{-1} mg^{-1}) was determined from a given surface area of membrane using the same experimental conditions.

2.5. Reusability and stability of the biocatalytic membranes

The reusability of the immobilized-trypsin membrane was evaluated by determining the biocatalytic membrane activity (Section 2.4) over several cycles at the optimal conditions found in Section 3.2.3 (i.e., pH 8 and temperature of 50 °C). After each cycle of enzymatic reaction with BAPNA solution, the bioactive composite membrane was removed from the solution and washed several times with trizma-HCl buffer solution before repeating the enzymatic reaction. Before the first cycle, the immobilized trypsin was assigned a relative activity of 100%.

Storage stability of both free-floating trypsin in solution and trypsin-immobilized membrane was tested for 14 days by determining the activity every day using the activity assay procedure described above at pH 8 and a temperature of 50 °C. Between measurements, trypsin solutions and membranes were kept in trizma-HCl buffer solution at 4 °C.

2.6. Performance tests of biocatalytic membranes

Performance tests of the biocatalytic membranes were carried out using a bench-scale cross-flow filtration system (total membrane surface area of 20.02 cm^2) to determine water flux and rejection of salts (NaCl, $MgCl_2$, Na_2SO_4, and $MgSO_4$) and BSA. The feed solution for the organic fouling studies was comprised of Na_2SO_4 (2 mM) and BSA (100 mg/L) in deionized water at pH 8.0. Prior to filtration, the membranes were compacted overnight under a pressure of 6.9 bar (100 psi). Filtration was performed under a pressure of 1.7 bar (25 psi). The cross-flow velocity was 21.4 cm/s. Temperature was maintained at a constant 25 ± 0.1 and 40 ± 0.2 °C for the filtration tests described in Sections 3.1 and 3.3, respectively. Protein solution flux (J_p) was recorded over 24 h using a logging device (FlowCal 5000). Feed and permeate were collected for salts and BSA measurement. Salt conductivity was measured with a bench-top conductivity meter (Oakton CON 2700).

The protein content was measured according to Micro BCA™ Protein Assay Reagent Kit (Thermo Fisher Scientific). BSA was used as a standard, with results expressed in mg equivalent of BSA per liter. A UV–vis spectrophotometer (Varian Carry 50 Bio) was used to determine the concentrations of protein at a wavelength of 592 nm.

To evaluate the antifouling property of the membranes, the flux decline rate (R_{fd}) was calculated by Eq. (2).

$$R_{fd} = \left[1 - \frac{J_p}{J_w}\right] \times 100 \quad (2)$$

where J_p is the steady state water flux in the presence of protein foulants and J_w is the pure water flux.

3. Results and discussion

3.1. Optimization of salt and protein rejection by LbL modified membranes

3.1.1. Effect of polyelectrolyte type on salt and protein rejection

The type of polyelectrolyte (PE) plays an important role in salt and protein rejection by influencing the thickness, pore size, and charge of the modified membranes [43]. In this study, PDADMAC, PEI, PAA, and PSS were explored for their effect on the efficiency of salt and protein (BSA) rejection (Fig. 2a).

In general, sulfate-based salts were rejected more favorably than chloride-based salts, while sodium-based salts were rejected more favorably than magnesium-based salts, suggesting that both size (steric)- and Donnan (charge)-exclusion mechanisms affect the rejection of salts by the PE membranes. The highest rejections of 5.2 ± 2.6%, 33.0 ± 0.6%, 36.9 ± 5.3%, and 81.8 ± 2.2% for $MgCl_2$, NaCl, $MgSO_4$, and Na_2SO_4, respectively, were achieved by the PDADMAC-PSS membrane, which especially excelled over other membranes in the rejection of Na_2SO_4. The lowest rejections of 4.1 ± 2.8%, 14.1 ± 1.5%, 2.9 ± 2.0%, and 6.9 ± 0.4% for $MgCl_2$, NaCl, $MgSO_4$, and Na_2SO_4, respectively, were achieved by the PDADMAC-PAA membrane. BSA, with a much larger molecular weight (66 kDa) than the salts used, was completely rejected by all modified membranes.

The higher rejection and lower permeability of PSS-terminated membrane compared to PAA-terminated membrane can be attributed to both size and charge effects. First, PSS deposition results in a thicker, more thorough coverage of the membrane surface and pores compared to PAA deposition, presumably due to the higher in-pore swelling of PSS compared to PAA [44–47]. Second, PSS is a strong polyelectrolyte (fully charged in solution) whereas PAA is weak polyelectrolyte (partially charged), leading to stronger Donnan exclusion of ions by PSS compared to PAA.

3.1.2. Effect of number of polyelectrolyte bilayers on salt and protein rejection

PDADMAC-PSS membrane was selected for further study to provide maximum rejection of salt. PSf substrate was covered with different numbers of PDADMAC-PSS bilayers (2, 4, or 6) to investigate the effect of number of PDADMAC-PSS bilayers on the rejection of salt and BSA (Fig. 2b). A significant increase in $MgSO_4$ rejection was observed with increasing number of bilayers from 2 to 4, presumably due to a narrowing of the membrane pore size. Further increase of the number of

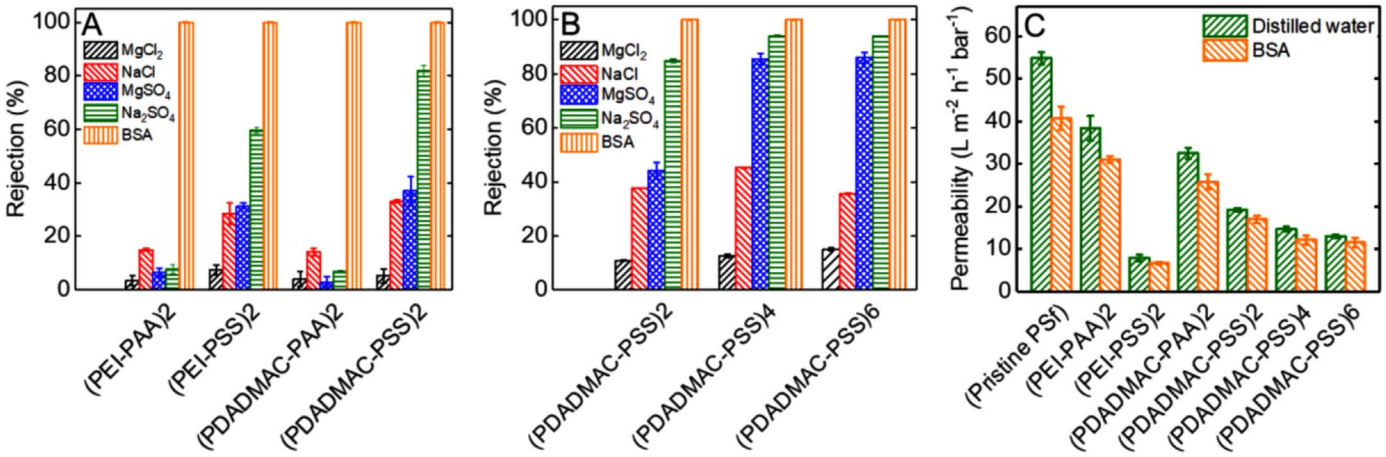

Fig. 2. (A) Effect of polyelectrolyte type on salt and BSA rejection. Experimental conditions: number of polyelectrolyte bilayers, 2; polyelectrolyte concentration, 500 ppm; salt concentration, 2 mM; BSA concentration, 100 mg/L; operating pressure, 1.7 bar (25 psi); filtration time, 1 h; cross-flow velocity, 21.4 cm/s; temperature, 25 ± 0.1 °C **(B)** Effect of number of polyelectrolyte bilayers (2, 4, or 6) on salt and BSA rejection. Experimental conditions: polyelectrolyte type, PDADMAC/PSS; polyelectrolyte concentration, 500 ppm; salt concentration, 2 mM; BSA concentration, 100 mg/L; operating pressure, 1.7 bar (25 psi); filtration time, 1 h; cross-flow velocity, 21.4 cm/s; temperature, 25 ± 0.1 °C. **(C)** Pure water flux and water flux with BSA solution for the various membranes. Experimental conditions: BSA concentration, 100 mg/L; pH, 6.28 ± 0.01; operating pressure 1.7 bar (25 psi); filtration time, 1 h; cross-flow velocity, 21.4 cm/s; temperature, 25 ± 0.1 °C.

bilayers from 4 to 6 did not improve rejection, suggesting that 4 bilayers fully covered the substrate membrane pores, with the minimum possible effective pore size reached. This pore size limit exists because of steric hindrance during deposition and repulsion of like-charged polymer strands. For comparison, Malaisamy et al. prepared LbL assembled PDADMAC—PSS bilayers on a commercial polyamide nanofiltration membrane and measured the monovalent anion selectivity of these composite membranes. The rejection of the resulting membranes to Cl^- increased from 30% to 91% after 8-bilayer modification, and the water flux decreased by 30% [48].

The rejection order of various salts by the PDADMAC-PSS composite membrane ($Na_2SO_4 > MgSO_4 > NaCl > MgCl_2$) matches the order previously reported for amphoteric composite NF membranes [49]. The negatively charged membrane surface strongly repulses multivalent anions (SO_4^{2-}) and strongly attracts multivalent cations (Mg^{2+}), while it exerts weaker forces on monovalent anions (Cl^-) and monovalent cations (Na^+) [50–52]. Typically, the Mg^{2+} is rejected better than Na^+ by NF membranes due to the steric-hindrance effect [53]. Here, the highest salt rejection of Na_2SO_4 and lowest salt rejection of $MgCl_2$ suggest that the Donnan (charge)-exclusion mechanism, not only the size (steric)-exclusion mechanism, plays an important role in the rejection mechanism of the PDADMAC-PSS membranes. The higher rejection of Na_2SO_4 compared to $MgSO_4$ was also reported by Lai et al. [54].

3.1.3. Effect of polyelectrolyte type and number of bilayers on membrane permeability

The permeability of deionized water and BSA solutions through different LbL modified membranes was measured (Fig. 2c). The pure water permeability was 55 ± 1.4, 38 ± 2.8, 32 ± 1.3, 19 ± 0.4, and 8 ± 0.7 L m^{-2} h^{-1} bar^{-1} for pristine PSf and 2 bilayers- PEI-PAA, PDADMAC-PAA, PDADMAC-PSS, and PEI-PSS membranes, respectively. The results indicate that the polyelectrolytes formed a thin film layer on the membrane surface, resulting in additional hydraulic resistance and flux decrease for all modified membranes. The higher water permeabilities for PAA-terminated membranes compared to PSS-terminated membranes can be attributed to the in-pore swelling of PSS, as discussed in Section 3.1.1. The pure water permeability was 19 ± 0.4, 14 ± 0.6, and 13 ± 0.4 L m^{-2} h^{-1} bar^{-1} for PDADMAC-PSS with 2, 4, and 6 bilayers, respectively. With increasing number of bilayers, the LbL assembly of PDADMAC-PSS reduced the membrane pore size and increased the thickness of the polyelectrolyte thin film, resulting in lower water flux.

When compared to deionized water permeability, BSA filtration caused a water flux decline due to protein-membrane interaction and adsorption of protein molecules on the membrane surface [55]. The adsorption of the BSA molecules to the membrane surface can be explained as the BSA (isoelectric point at pH 4.7) was not completely negatively charged at the feed solution pH tested (6.3), resulting in decreased electrostatic repulsion between BSA molecules and the membrane surface. Also, an attraction between the negatively charged BSA molecules to locally uncharged or positively charged regions on the membrane surface can occur. The PSS polyanion showed better antifouling characteristics with lower flux decline compared to the PAA polyanion, suggesting that PAA-BSA interaction was stronger than PSS-BSA interaction. This observation can be attributed to higher electrostatic repulsion between PSS and the BSA molecule compared to the repulsion between PAA and BSA molecule due to the lower pKa value of PSS than PAA, with the corresponding higher negative charge of PSS at a given pH.

3.2. Characterization and optimization of the biocatalytic membranes

Following the optimization of salt and BSA rejection, the PDADMAC-PSS membrane with 4 bilayers was chosen as the platform for further study and optimization of trypsin immobilization and biocatalytic activity.

3.2.1. ATR-FTIR spectra, hydrophilicity, and roughness of the biocatalytic membranes

The chemical bonds at the surface of trypsin powder and pristine PSf, PDADMAC-PSS-TRY (Fig. 1a), and PSS-PAH-GA-TRY (Fig. 1b) membranes were characterized using ATR-FTIR spectroscopy (Fig. 3). Trypsin powder showed bands at 1635, 1550, and 3300 cm^{-1}, indicating the vibrations corresponding to amide I (C=O), amide II (N-H), and primary amine bands of protein molecules. C–H and N–H bands were observed between 2930 cm^{-1} and 3300 cm^{-1}, respectively, because of stretching vibrations. In the ATR-FTIR spectrum for the pristine PSf membrane, the band at 1150 cm^{-1} was the characteristic band of the S=O symmetric group of sulfone. The bands observed at 1320 cm^{-1} and 1240 cm^{-1} are attributed to the C-SO_2-C and C-O asymmetric stretch, respectively. The C_6H_6 ring stretch and CH_3 groups of PSf showed a band at 1583 cm^{-1} and 2870 cm^{-1}, respectively. After trypsin immobilization, 1655 cm^{-1} (NH_2, primary amine), 2930 cm^{-1}

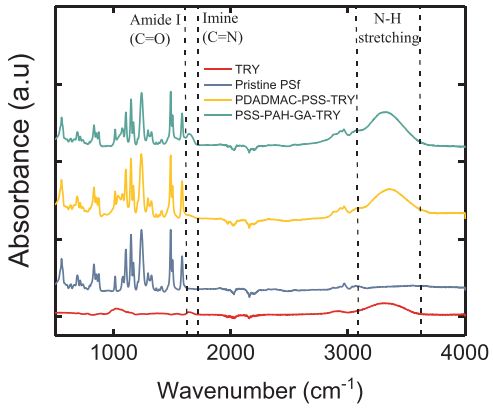

Fig. 3. ATR-FTIR spectra of trypsin powder and pristine PSf, PDADMAC-PSS-TRY, and PSS-PAH-GA-TRY membranes. Conditions during membrane preparation: 4 PDADMAC-PSS bilayers, 500 mg/L polyelectrolyte (PDADMAC, PSS, PAH) solutions, incubation with trypsin for 24 h at 25 ± 0.1 °C.

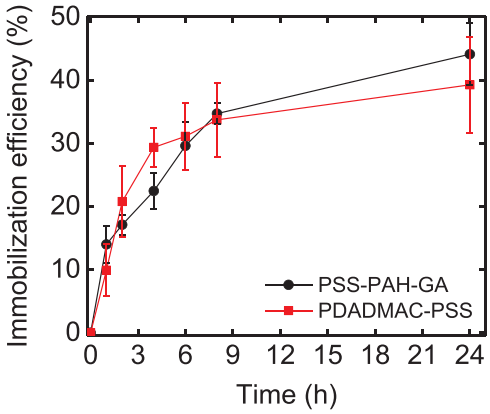

Fig. 4. Effect of immobilization time for trypsin enzyme on the immobilization efficiency of PSS-PAH-GA and PDADMAC-PSS membranes. Experimental conditions: enzyme concentration, 1 mg/mL; vessel volume, 100 mL; buffer, Trizma-HCl, 0.1 M, pH 8.0; stirring rate, 250 rpm; temperature, 25 ± 0.1 °C; membrane area, 60 cm^2. The amount of immobilized trypsin on the membranes after 24 h was 5.64 and 6.78 mg enzyme/g membrane for PDADMAC-PSS and PSS-PAH-GA membranes, respectively.

(C-H) and 3350 cm^{-1} (NH, OH groups) were observed for both PDADMAC-PSS-TRY and PSS-PAH-GA-TRY membranes. A minor C=N stretch was observed at 1677 cm^{-1} for the PSS-PAH-GA-TRY membrane, attributed to the Schiff-based reaction between amine and aldehyde groups. The OH aliphatic stretch at 2970 cm^{-1} was detected for trypsin powder and PDADMAC-PSS-TRY and PSS-PAH-GA-TRY membranes.

The contact angle of the modified membranes is summarized in Table S1. All modified membranes presented lower contact angle compared to the pristine membrane, suggesting that the fabricated membranes were more hydrophilic than the PSf pristine membrane. PEI-PAA and PEI-PSS modified membranes exhibited the lowest (i.e., most hydrophilic) and highest (i.e., most hydrophobic) contact angles, respectively. This finding suggests that the lower water permeability observed for the PEI-PSS modified membranes compared to other membranes (Fig. 2c) is due to the better coverage of the PSf membrane by PSS compared to the other polyelectrolytes. Additionally, the hydrophilicity increased when the number of polyelectrolyte bilayers increased from 2 to 4 but did not increase with further increase in the number of polyelectrolyte bilayers, supporting the results in Fig. 2b that 4 bilayers fully covered the substrate membrane.

AFM analyses were used to characterize the surface roughness of the pristine and modified NF membranes (Fig. S4). The bright and dark regions show the highest points and the pores of the membrane surface, respectively. The AFM images and the average surface roughness (*Ra*) (Table S1) indicate that the surface roughness of the polyelectrolyte-modified membranes is higher than that of pristine PSf membrane (Fig. S4). Different polyelectrolytes led to varying degrees of roughness of the membrane surfaces due to the different chemical structures of the polyelectrolytes and their complexation with the membrane surface. Importantly, since membrane fouling is more easily formed on rough membranes than on smooth membranes [56], TRY-immobilized membranes with lower roughness can potentially provide better antifouling performance compared to LbL-modified NF membranes without TRY.

3.2.2. *Effect of immobilization time on immobilization efficiency*

The effect of immobilization time of trypsin using PDADMAC-PSS and PSS-PAH-GA membranes was measured at room temperature and pH 8 with initial trypsin concentration of 1 mg/mL (Fig. 4). The immobilization efficiency (IE) was determined using

$$IE = \frac{(C_i - C_e)}{C_i} \times 100\% \quad (3)$$

where C_i (mg mL^{-1}) is the initial protein concentration in solution and C_e (mg mL^{-1}) is the protein concentration after the specific immobilization time indicated.

Trypsin loading on both membranes increased rapidly during the initial 9 h, after which the loading rate decreased significantly, exhibiting a classic second-order rate curve. This behavior is reasonable considering that the adsorption rate depends on both the number of available adsorption sites and the concentration of enzyme. After 24 h, the immobilization efficiency of PSS-PAH-GA membrane (44.1 ± 4.9%) was higher than that of PDADMAC-PSS membrane (39.2 ± 7.6%), due to the covalent bonding of the enzyme with GA.

3.2.3. *Effect of pH and temperature on the biocatalytic activity*

The relative activity of the free and immobilized trypsin on the PDADMAC-PSS and PSS-PAH-GA membranes was explored as a function of pH and temperature (Fig. 5) using the conditions described in Table 2. For both free and immobilized enzyme, the trypsin enzyme was active in the pH range of 5–12, with an optimum at pH 8 (Fig. 5a). The activity of trypsin was found to increase proportionally with the increase in pH from 5 to 8 and drop beyond pH 9. Regardless of immobilization type (electrostatic with PSS or covalent with GA), a pH of 8 was optimal for enzyme activity. This value of pH also matches the findings of Kamburov and Lalov when immobilizing trypsin onto chitosan gel macro beads pre-activated with glutaraldehyde [57]. At higher pH range (9–12), the immobilized enzyme showed higher activity than free enzyme, and higher enzyme activity was observed for the PSS-PAH-GA-TRY membrane at pH > 9 than for the PDADMAC-PSS-TRY membrane. Multipoint covalent bonding of trypsin to a substrate has previously been shown to protect against denaturation at high pH. Electrostatic attraction would somewhat protect against denaturation but is more easily broken at higher pH. For both membrane types with trypsin as well and as free-floating trypsin, the lower activity at low pH can be attributed to the competitive bonding of protons with the aspartate within trypsin. This residue is responsible for attracting and stabilizing positive arginine and lysine residues in other proteins before the enzyme cleaves them [58,59].

Immobilization had no effect on the optimal temperature (50 °C) for the PDADMAC-PSS-TRY membrane but increased the optimal temperature (60 °C) for the PAH-GA-TRY membrane (Fig. 5b). The difference in optimal temperature might be due to higher activation energy for covalently-bonded trypsin since energy is distributed into the covalent bond. The results showed that PAH-GA-TRY and PDADMAC-PSS-TRY membranes were more stable at high temperatures above 70 °C. Normally, enzymes are denatured when the temperature exceeds 60 °C, whereas in our study the covalently immobilized enzymes were heat resistant. The same phenomenon was observed by Kamburov and Lalov [57]. On the other hand, Johnson and Makame [60] covalently

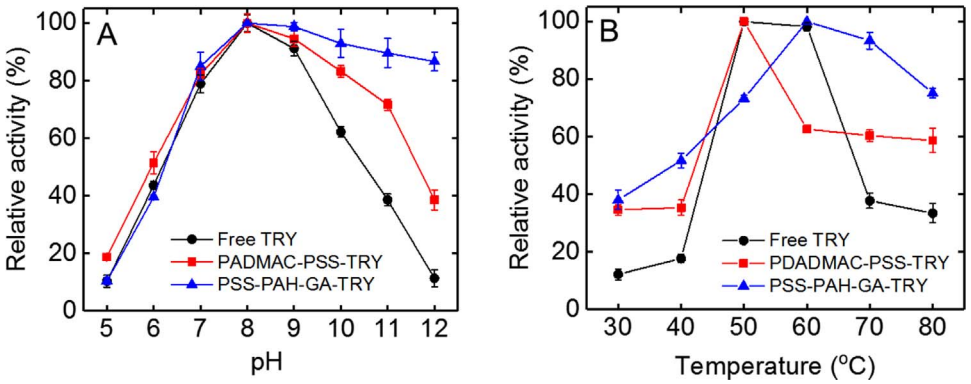

Fig. 5. (A) pH variation of the relative activity for free TRY and PDADMAC-PSS-TRY and PSS-PAH-GA-TRY membranes. Experimental conditions: reaction volume, 10 mL; temperature, 30 °C; reaction time, 30 min; stirring rate, 250 rpm; membrane area, 9 cm^2. **(B)** Temperature variation of the relative activity for free TRY, PDADMAC-PSS-TRY, and PSS-PAH-GA-TRY membranes. Experimental conditions: reaction volume, 10 mL; pH, 8.0; time, 30 min; stirring rate, 250 rpm; membrane area, 9 cm^2.

immobilized bovine pancreatic trypsin onto monolithic polyacrylamide cryogels with epoxy functionality and reported an optimal temperature of 50 °C for both immobilized and free trypsin.

3.2.4. *Reusability and storage stability of the biocatalytic membrane*

The reusability and storage stability of the biocatalytic membranes were tested in subsequent cycles for the hydrolysis of BAPNA as described in Section 2.5. Both PDADMAC-PSS-TRY and PSS-PAH-GA-TRY membranes showed decreased trypsin activity as the reuse number increased (Fig. 6a). After ten cycles (5 h), the PDADMAC-PSS-TRY membrane significantly lost its activity while the PSS-PAH-GA-TRY membrane maintained almost 80% of its initial activity. We attribute the lower preservation of enzyme activity for the PDADMAC-PSS-TRY membrane to the weaker electrostatic interaction between the sulfone and amine groups compared to the covalent binding between aldehyde and amine groups on the PSS-PAH-GA-TRY membrane. Li et al. reported that the adsorbed trypsin in Mesoporous Silica SBA-15 retained only 42% of its initial activity after seven cycles. Similarly, they attributed the loss of enzyme activity to the leaching of adsorbed trypsin at the repeated reaction, owing to the weak electrostatic interaction between trypsin and mesoporous silica SBA-15 [61].

The free and immobilized enzymes were tested for storage stability (Fig. 6b). They were kept 14 days at 4 °C, and the enzyme activity was determined daily using the standard activity assay described above. Under the same conditions, free enzyme and PDADMAC-PSS-TRY retained only 38.1 ± 1.3% and 42.2 ± 2.1%, respectively, of their initial activity during 14 days of storage compared to 69.73 ± 4.6% for the PSS-PAH-GA-TRY membrane. This enhanced stability of the PSS-PAH-GA-TRY membrane can be related to the prevention of enzyme autolysis after covalently bonding enzyme on the membrane and is comparable with previous studies [61–64].

3.3. *Protein fouling behavior of LbL modified and biocatalytic membranes*

Membrane performance was evaluated in terms of permeate water flux and rejection of salt and BSA (Fig. 7). LbL-modified membranes without trypsin were fouled easily by BSA, as indicated by the steep decline in permeation water flux over time (Fig. 7a). Although electrostatic repulsion between the negatively charged BSA (IEP at pH 4.7) and PSS outer layer would be expected, BSA was adsorbed to the PDADMAC-PSS membrane. Adsorption of protein molecules on the membrane surface can be explained by the heterogeneous surface charge of BSA proteins as well as the acidic groups present on the PDADMAC-PSS membrane surface that can alter the BSA tertiary structure, giving rise to surface adsorption [65,66]. In the case of the PSS-PAH-GA, we attribute the flux deterioration to weak interactions between aldehyde and BSA molecules.

Trypsin immobilization on the PDADMAC-PSS-TRY and the PSS-PAH-GA-TRY membranes resulted in lower fouling and minimal flux decline compared to the PDADMAC-PSS and the PSS-PAH-GA membranes by protecting the membrane surface from BSA adsorption. The PSS-PAH-GA-TRY membrane exhibited superior fouling resistance, which is attributed to the increased biocatalytic activity of the covalently immobilized enzyme. The PDADMAC-PSS, PSS-PAH-GA, PDADMAC-PSS-TRY, and PSS-PAH-GA-TRY membranes showed R_{fd} values of 22.86%, 20.83%, 11.53%, and 8.45%, respectively (Fig. 7b), indicating higher resistance to protein fouling of the trypsin-immobilized membranes compared to the membranes with only LbL-modification. Moreover, high rejection of BSA and Na_2SO_4 was observed for all membranes, and biocatalytic membrane activity was not affected in the presence of salt.

4. Conclusion

Layer-by-layer self-assembly of polyelectrolytes was used for trypsin immobilization on a PSf UF support to obtain a biocatalytic NF membrane. Membranes were modified with PDADMAC/PAA or PDADMAC/PSS bilayers, showing that a PSS-based multilayer polyelectrolyte film provided higher salt rejection than a PAA-based multilayer polyelectrolyte film. Trypsin enzyme was successfully immobilized

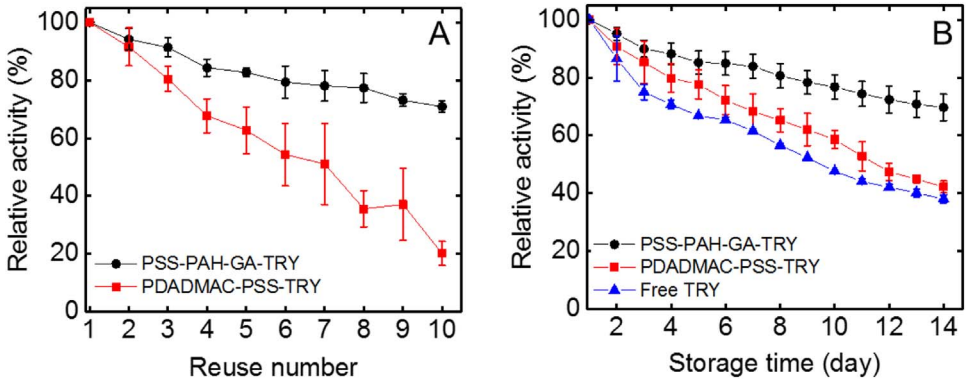

Fig. 6. (A) Relative activity as a function of reuse number for the PSS-PAH-GA-TRY and PDADMAC-PSS-TRY membranes. Each cycle lasted 30 min **(B)** Relative activity as a function of storage stability for the PSS-PAH-GA-TRY and PDADMAC-PSS-TRY membranes as well as free TRY. Experimental conditions: reaction volume, 10 mL; pH, 8.0; temperature, 50 °C; reaction time, 30 min. The specific activity of free TRY, PDADMAC-PSS-TRY membrane, and PSS-PAH-GA-TRY membrane were 167.7, 13.5, and 11.2 μmol min^{-1} g^{-1}, respectively. The first cycle was taken as the control (100%).

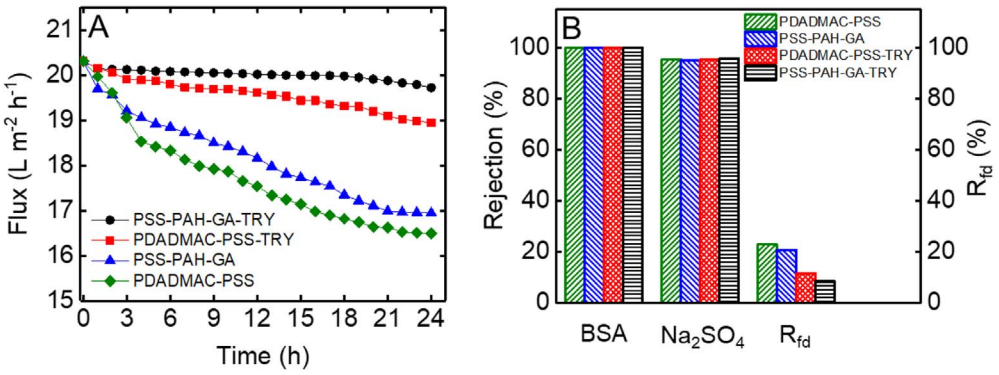

Fig. 7. (A) Water flux of the LbL modified membranes before and after trypsin immobilization for the PDADMAC-PSS-TRY, PSS-PAH-GA-TRY, PDADMAC-PSS, and PSS-PAH-GA membranes. Experimental conditions: initial flux, 20.31 L m^{-2} h^{-1}; cross-flow velocity, 21.4 cm/s; Na_2SO_4 concentration, 2 mM; BSA concentration, 100 mg/L; pH 8.0 ± 0.2; temperature, 40 ± 0.1 °C; filtration time, 24 h. **(B)** Rejection and flux decline ratio (R_{fd}) values before and after trypsin immobilization. Experimental conditions: initial flux, 20.31 L m^{-2} h^{-1}; cross-flow velocity, 21.4 cm/s; Na_2SO_4 concentration, 2 mM; BSA concentration, 100 mg/L; pH 8.0 ± 0.2; temperature, 40 ± 0.1 °C; filtration time, 24 h.

electrostatically on the negatively charged PDADMAC-PSS membrane surface or bounded covalently with PAH using glutaraldehyde (GA) as a cross-linker. Optimal pH and temperature for TRY activity were determined as 8 and 50 °C, respectively. The optimal temperature was shifted to 60 °C after trypsin immobilization on the PSS-PAH-GA membrane. The PDADMAC-PSS-TRY and PSS-PAH-GA-TRY membranes conserved 42.2 ± 2.1 and 69.73 ± 4.6% of the initial activity after 14 days, respectively. Flux decline rate (R_{fd}) values showed that trypsin-immobilized membranes have higher resistance to BSA fouling than the LbL modified membranes without enzyme. The antifouling resistance order of the membranes (PSS-PAH-GA-TRY > PDADMAC-PSS-TRY > PSS-PAH-GA > PDADMAC-PSS) shows the potential of enzyme immobilization on NF membrane via LbL self-assembly to prevent protein fouling on membrane surfaces in the presence of salt.

Acknowledgments

We acknowledge the Scientific and Technological Research Council of Turkey, the Department of Science Fellowships and Grant Programs (1059B191501137) for financially supporting Dr. Nadir Dizge. We also acknowledge the United States–Israel Binational Agricultural Research and Development Fund BARD, Fellowship number FI-549-2016, for providing the postdoctoral fellowship to Dr. Razi Epsztein.

Appendix A. Supplementary material

Supplementary data associated with this article can be found in the online version at http://dx.doi.org/10.1016/j.memsci.2017.12.026.

References

[1] N. Hilal, H. Al-Zoubi, A.W. Mohammad, N.A. Darwish, Nanofiltration of highly concentrated salt solutions up to seawater salinity, Desalination 184 (2005) 315–326.
[2] L.P. Raman, M. Cheryan, N. Rajagopalan, Consider nanofiltration for membrane separation, Chem. Eng. Prog. 90 (1994) 68–74.
[3] P. Eriksson, Nanofiltartion extends the range of membrane filtration, Environ. Prog. 7 (1988) 58–61.
[4] A.E. Childress, M. Elimelech, Relating nanofiltration membrane performance to membrane charge (electrokinetic) characteristics, Environ. Sci. Technol. 34 (17) (2000) 3710–3716.
[5] A. Szymczyk, P. Fievet, Ion transport through nanofiltration membranes: the steric, electric and dielectric exclusion model, Desalination 200 (2006) 122–124.
[6] A.G. Fane, C.Y. Tang, R. Wang, Membrane technology for water: microfiltration, ultrafiltration, nanofiltration, and reverse osmosis, in: P. Wilderer (Ed.), Treatise on Water Science, Academic Press, Oxford, 2011, pp. 301–335.
[7] J. Meier, T. Melin, Wastewater reclamation by the PAC-NF process, Desalination 178 (1–3) (2005) 27–40.
[8] E. Hassanzadeh, M. Farhadian, A. Razmjou, N. Askari, An efficient wastewater treatment approach for a real woolen textile industry using a chemical assisted NF membrane processy, Environ. Nanotechnol. Monit. Manag. 8 (2017) 92–96.
[9] L.D. Nghiem, A.I. Schäfer, M. Elimelech, Role of electrostatic interactions in the retention of pharmaceutically active contaminants by a loose nanofiltration membrane, J. Membr. Sci. 286 (2006) 52–59.
[10] Y. Wu, S. Xia, B. Dong, H. Chu, J. Liu, Study on surface water treatment by hybrid sand filtration and nanofiltration, Desalin. Water Treat. 51 (2013) 25–27.
[11] A.R. Costa, M.N. de Pinho, Performance and cost estimation of nanofiltration for surface water treatment in drinking water production, Desalination 196 (1–3) (2006) 55–65.
[12] D.J. Barker, S.M.L. Salvi, A.A.M. Langenhoff, D.C. Stuckey, Soluble microbial products in ABR treating low-strength wastewater, J. Environ. Eng. 126 (3) (2000) 239–249.
[13] C. Jarusutthirak, G. Amy, Role of soluble microbial products (SMP) in membrane fouling and flux decline, Environ. Sci. Technol. 40 (3) (2006) 969–974.
[14] N. Her, G. Amy, A. Plottu-Pecheux, Y. Yoon, Identification of nanofiltration membrane foulants, Water Res. 41 (17) (2007) 3936–3947.
[15] S. Boributh, A. Chanachai, R. Jiraratananon, Modification of PVDF membrane by chitosan solution for reducing protein fouling, J. Membr. Sci. 342 (2009) 97–104.
[16] G.B. Sigal, M. Mrksich, G.M. Whitesides, Effect of surface wettability on the adsorption of proteins and detergents, J. Am. Chem. Soc. 120 (1998) 3464–3473.
[17] F. Fang, I. Szleifer, Effect of molecular structure on the adsorption of protein on surfaces with grafted polymers, Langmuir 18 (2002) 5497–5510.
[18] I.H. Huisman, P. Prádanos, A. Hernández, The effect of protein–protein and protein–membrane interactions on membrane fouling in ultrafiltration, J. Membr. Sci. 179 (2000) 79–90.
[19] R. Miao, L. Wang, N. Mi, Z. Gao, T. Liu, Y. Lv, X. Wang, X. Meng, Y. Yang, Enhancement and mitigation mechanisms of protein fouling of ultrafiltration membranes under different ionic strengths, Environ. Sci. Technol. 49 (11) (2015) 6574–6580.
[20] S.T. Kelly, A.L. Zydney, Mechanisms for BSA fouling during microfiltration, J. Membr. Sci. 107 (1–2) (1995) 115–127.
[21] X. Wei, G. Li, J. Nie, H. Xiang, J. Chen, Preparation and improvement anti-fouling property and biocompatibility of polyethersulfone membrane by blending comb-like amphiphilic copolymer, J. Porous Mater. 21 (2014) 589–599.
[22] Y.N. Wang, C.Y. Tang, Protein fouling of nanofiltration, reverse osmosis, and ultrafiltration membranes—the role of hydrodynamic conditions, solution chemistry, and membrane properties, J. Membr. Sci. 376 (2011) 275–282.
[23] M.R. Mandavi, M. Delnavaz, V. Vatanpour, Fabrication and water desalination performance of piperazine-polyamide nanocomposite nanofiltration membranes embedded with raw and oxidized MWCNTs, J. Taiwan Inst. Chem. Eng. 75 (2017) 189–198.
[24] Q. Li, M. Elimelech, Natural organic matter fouling and chemical cleaning of nanofiltration membranes, Water Sci. Technol.: Water Supply 4 (5–6) (2005) 245–251.
[25] P. Le-Clech, V. Chen, T.A.G. Fane, Fouling in membrane bioreactors used in wastewater treatment, J. Membr. Sci. 284 (2006) 17–53.
[26] J.R. Cherry, A.L. Fidantsef, Directed evolution of industrial enzymes: an update, Curr. Opin. Biotechnol. 14 (2003) 438–443.
[27] S. Datta, L.R. Christena, Y. Rani, S. Rajaram, Enzyme immobilization: an overview on techniques and support materials, Biotechnology 3 (2013) 1–9.
[28] S. Guedidi, Y. Yurekli, A. Deratani, P. Déjardin, C. Innocent, S.A. Altinkaya, S. Roudesli, A. Yemenicioglu, Effect of enzyme location on activity and stability of trypsin and urease immobilized on porous membranes by using layer-by-layer self-assembly of polyelectrolyte, J. Membr. Sci. 365 (2010) 59–67.
[29] G. Decher, J.D. Hong, Buildup of ultrathin multilayer films by a self-assembly process, 1. Consecutive adsorption of anionic and cationic bipolar amphiphiles on charged surfaces, Makromol. Chem. Macromol. Symp. 46 (1991) 321–327.
[30] L. Krasemann, A. Toutianoush, B. Tieke, Self-assembled polyelectrolyte multilayer membranes with highly improved pervaporation separation of ethanol/water mixtures, J. Membr. Sci. 181 (2001) 221–228.
[31] G. Zhang, W. Gu, S. Ji, Z. Liu, Y. Peng, Z. Wang, Preparation of polyelectrolyte multilayer membranes by dynamic layer-by-layer process for pervaporation separation of alcohol/water mixtures, J. Membr. Sci. 280 (2006) 727–733.
[32] K. Yan, E. Laleh, M.J. Lee, D. Liu, B. Mi, layer-by-layer assembly of zeolite/polyelectrolyte nanocomposite membranes with high zeolite loading, Environ. Sci. Technol. Lett. 1 (2014) 504–509.
[33] J. Yanli, A. Quanfu, Z. Qiang, C. Huanlin, G. Congjie, Preparation of novel positively charged copolymer membranes for nanofiltration, J. Membr. Sci. 376 (2011) 254–265.
[34] N. Divya, D.G. Bhagat, B. Rahul, U.K. Kharul, In situ growth of metal-organic frameworks on a porous ultrafiltration membrane for gas separation, J. Mater. Chem. A 1 (2013) 8828–8835.
[35] W. Jin, A. Toutianoush, B. Tieke, Use of polyelectrolyte layer-by-layer assemblies as

nanofiltration and reverse osmosis membranes, Langmuir 19 (2003) 2550–2553.
[36] R.H. Lajimi, E. Ferjani, M.S. Roudesli, A. Deratani, Effect of LbL surface modification on characteristics and performances of cellulose acetate nanofiltration membranes, Desalination 266 (2011) 78–86.
[37] R. Malaisamy, M.L. Bruening, High-flux nanofiltration membranes prepared by adsorption of multilayer polyelectrolyte membranes on polymeric supports, Langmuir 21 (2005) 10587–10592.
[38] L. Krasemann, B. Tieke, Selective ion transport across self-assembled alternating multilayers of cationic and anionic polyelectrolytes, Langmuir 16 (2000) 287–290.
[39] L. Ouyang, R. Malaisamy, M.L. Bruening, Multilayer polyelectrolyte films as nanofiltration membranes for separating monovalent and divalent cations, J. Membr. Sci. 310 (2008) 76–84.
[40] Z. Yin, W. Zhao, M. Tian, Q. Zhang, L. Guo, L. Yang, A capillary electrophoresis-based immobilized enzyme reactor using graphene oxide as a support via layer by layer electrostatic assembly, Analyst 139 (2014) 1973–1979.
[41] Y. Liu, H. Lu, W. Zhong, P. Song, J. Kong, P. Yang, H.H. Girault, B. Liu, Multilayer-assembled microchip for enzyme immobilization as reactor toward low-level protein identification, Anal. Chem. 78 (2006) 801–808.
[42] A. Schulze, A. Stoelzer, K. Striegler, S. Starke, A. Prager, Biocatalytic self-cleaning polymer membranes, Polymers 7 (2015) 1837–1849.
[43] V. Smuleac, D.A. Butterfield, D. Bhattacharyya, Layer-by-Layer-assembled microfiltration membranes for biomolecule immobilization and enzymatic catalysis, Langmuir 22 (2006) 10118–10124.
[44] J.B. Schlenoff, S.T. Dubas, Mechanism of polyelectrolyte multilayer growth: charge over compensation and distribution, Macromolecules 34 (2001) 592–598.
[45] J. de Grooth, M. Dong, W.M. de Vos, K. Nijmeijer, Building poly zwitterion-based multilayers for responsive membranes, Langmuir 30 (2014) 5152–5161.
[46] M.L. Bruening, M. Adusumilli, Polyelectrolyte multilayer films and membrane functionalization, Mater. Matters 6 (2011) 76–81.
[47] J. de Grooth, R. Oborný, J. Potreck, K. Nijmeijer, W.M. de Vos, The role of ionic strength and odd–even effects on the properties of polyelectrolyte multilayer nanofiltration membranes, J. Membr. Sci. 475 (2015) 311–319.
[48] R. Malaisamy, A. Talla-Nwafo, K.L. Jones, Polyelectrolyte modification of nanofiltration membrane for selective removal of monovalent anions, Sep. Purif. Technol. 77 (2011) 367–374.
[49] J. Miao, H. Lin, W. Wang, L.C. Zhang, Amphoteric composite membranes for nanofiltration prepared from sulfated chitosan crosslinked with hexamethylene diisocyanate, Chem. Eng. J. 234 (2013) 132–139.
[50] M.R. Teixeira, M.J. Rosa, M. Nystrom, The role of membrane charge on nanofiltration performance, J. Membr. Sci. 265 (2005) 160–166.
[51] A.M. Urtiaga, I. Ortiz, J.A. Irabien, Nanofiltration separation of polyvalent and monovalent anions in desalination brines, J. Membr. Sci. 473 (2015) 16–27.
[52] N. Pages, A. Yaroshchuk, O. Gibert, J.L. Cortina, Rejection of trace ionic solutes in nanofiltration: influence of aqueous phase composition, Chem. Eng. Sci. 104 (2013) 1107–1115.
[53] D.X. Wang, M. Su, Z.Y. Yu, X.L. Wang, M. Ando, T. Shintani, Separation performance of a nanofiltration membrane influenced by species and concentration of ions, Desalination 175 (2005) 219–225.
[54] G.S. Lai, W.J. Lau, P.S. Goh, A.F. Ismail, N. Yusof, Y.H. Tan, Graphene oxide incorporated thin film nanocomposite nanofiltration membrane for enhanced salt removal performance, Desalination 387 (2016) 14–24.
[55] D. Breite, M. Went, I. Thomas, A. Prager, A. Schulze, Particle adsorption on a polyether sulfone membrane: how electrostatic interactions dominate membrane fouling, RSC Adv. 6 (2016) 65383–65391.
[56] E.M. Virijenhoek, S. Hong, M. Elimelech, Influence of membrane surface properties on initial rate of colloidal fouling of reverse osmosis and nanofiltration membranes, J. Membr. Sci. 188 (2001) 115–128.
[57] M. Kamburov, I. Lalov, Preparation of chitosan beads for trypsin immobilization, Biotechnol. Biotechnol. EQ. 26/2012/SE, Special Edition/On-Line.
[58] J.C.S. dos Santos, N. Rueda, O. Barbosa, M.C. Millán-Linares, J. Pedroche, M.M. Yuste, L.R.B. Gonçalves, R. Fernandez-Lafuente, Bovine trypsin immobilization on agarose activated with divinylsulfone: improved activity and stability via multipoint covalent attachment, J. Mol. Catal. B: Enzym. 117 (2015) 38–44.
[59] C.S. Craik, S. Roczniak, C. Largman, W.J. Rutter, The catalytic role of the active site aspartic acid in serine proteases, Science 21 (4817) (1987) 909–913 (237).
[60] W. Johnson, Y.M.M. Makame, Activity of enzyme trypsin immobilized onto macroporous poly(epoxy-acrylamıde) cryogel, Tanz. J. Sci. 38 (3) (2012) 54–64.
[61] S. Li, Z. Wu, M. Lu, Z. Wang, Z. Li, Improvement of the enzyme performance of trypsin via adsorption in mesoporous Silica SBA-15: hydrolysis of BAPNA, Molecules 18 (2013) 1138–1149.
[62] F. Xu, W.H. Wang, Y.J. Tan, M.L. Bruening, Facile trypsin immobilization in polymeric membranes for rapid, efficient protein digestion, Anal. Chem. 82 (24) (2010) 10045–10051.
[63] J. Qiao, J.Y. Kim, Y.Y. Wang, L. Qi, F.Y. Wang, M.H. Moon, Trypsin immobilization in ordered porous polymer membranes for effective protein digestion, Anal. Chim. Acta 906 (2016) 156–164.
[64] G. Cheng, S.Y. Zheng, Construction of a high-performance magnetic enzyme nanosystem for rapid tryptic digestion, Sci. Rep. 4 (6947) (2014) 1–10.
[65] C.L. Cooper, P.L. Dubin, A.B. Kayitmazer, S. Turksen, Polyelectrolyte–protein complexes, Curr. Opin. Colloid Interface Sci. 10 (2005) 52–78.
[66] S.F. Oppenheim, J.O. Rich, G.R. Buettner, V.G.J. Rodgers, Protein structure change on adherence to ultrafiltration membranes: an examination by electron paramagnetic resonance spectroscopy, J. Colloid Interface Sci. 183 (1996) 274–279.